CrystEngComm

Accepted Manuscript

Single-Step Synthesis and Catalytic Activity of Structure-Controlled Nickel Sulfide Nanoparticles

Rajan Karthikeyan,[†] Dheivasigamani Thangaraju,[‡] Natarajan Prakash,[†] and Yasuhiro Hayakawa[†,‡,*]

[†]Graduate School of Science and Technology, Shizuoka University, 3-5-1 Johoku, Naka-ku, Hamamatsu, Shizuoka 432-8011, Japan

[‡]Research Institute of Electronics, Shizuoka University, 3-5-1 Johoku, Naka-ku, Hamamatsu, Shizuoka 432-8011, Japan

*Corresponding author. Tel./Fax: +81 53 478-1310

E-mail: royhaya@ipc.shizuoka.ac.jp (Yasuhiro Hayakawa)

Single-Step Synthesis and Catalytic Activity of Structure-Controlled Nickel Sulfide Nanoparticles

ABSTRACT

Nanoparticle single-phase nickel sulfides such as NiS, NiS_2, Ni_3S_4, and Ni_7S_6 were prepared from elemental sulfur and nickel nitrate hexahydrate, using a temperature-controlled precursor injection method. The initial ratio of the concentrations of the sources was used to control the size and phase of the final product. Phase control was confirmed using X-ray diffraction and transmission electron microscopy. The synthesized nickel sulfide phases, which had metallic characteristics, were used to study the catalytic reduction of 4-nitrophenol. The results showed that the catalytic activity of the NiS nanoparticles in the reduction of 4-nitrophenol to 4-aminophenol was higher than those of the other nickel sulfide phases. In addition, the nanocrystals showed good separation ability and reusability for reduction of 4-nitrophenol.

INTRODUCTION

Inorganic nanoparticle synthesis has received much attention for optical, electrical, and magnetic applications due to its rich physico-chemical properties. Environmental friendly transition metal chalcogenide nanoparticle synthesis is the current interest in energy applications[1–4]. Nickle sulfides have potential applications in lithium ion batteries, supercapacitors, and dye-sensitized solar cells[5–7]. The different phases of nickle sulfide has more complex phases such as NiS (α-NiS and β-NiS), Ni_3S_2, NiS_2, Ni_3S_4, Ni_9S_8, and Ni_7S_6 make synthesis of single-phase nickel sulfide complicated. The phase diagram of nickel sulfide has a large number of sulfur-rich and nickel-rich phases at low temperatures. The synthesis of sulfur-rich phases is less complex than that of nickel-rich phases. NiS shows two different phase types, depending on the synthesis temperature. Kullerud and Yund reported that the phase transformation from α-NiS to β-NiS occurs at 282 °C[8].

Nickel sulfides with different phases and morphologies, such as layer-rolled NiS[9], hexagonal NiS[10–13], NiS_2 cuboids, NiS nanobelts[14], three-dimensional flower-like rhombohedral NiS, and dodecahedral NiS_2[15] have been synthesized, using different methods, for various applications; for example, NiS_2 cubic nanoparticles have been used for photocatalytic hydrogen production and in supercapacitors[16]. Several methods for the synthesis of selenide[1] and sulfide[3,17] nanocrystals have been investigated. Solvothermal and wet-chemical methods[18], which involve high-temperature solid-state and vapor-phase reactions, have been used to synthesize nickel sulfides. However, controlled-phase nickel sulfide synthesis is difficult using these methods. In hydrothermal or solvothermal synthesis, concentration control leads to the formation of

other phases within the synthesized product[19]. The synthesis of nickel sulfide phases such as Ni_3S_4 requires a two-step reduction process[20] to control the phase and morphology. We have developed a single-step injection process, using oleylamine as both the solvent and the reducing agent, to obtain the desired phases in the nickel sulfide binary phase diagram. We described the synthesis and evolution of hierarchical nickel sulfide architectures in our previous communication[19].

Temperature-controlled injection reactions have several advantages in the synthesis of nanoparticles, such as low cost and better productivity[21]. Shape control of sulfur-based nanocrystals by injecting a molecular precursor into high-boiling-point solvents was reported by Lee et al[22]. Recently, many groups have focused on using different amines for the size- and structure-controlled synthesis of individual metal sulfide phases[2,23–25]. The use of oleylamine–metal complexes has been well studied by Joo et al.; they reported the synthesis of various size-controlled metal sulfides such as PbS, ZnS, CdS, and MnS, with particle sizes of 6−13 nm[26]. Sulfur–oleylamine interactions lead to the formation of H_2S, which reacts with a metal precursor to form metal sulfide nanoparticles[24].

In this paper, we describe the single-step, structure-controlled synthesis of nickel sulfide nanoparticles with different phases, using a precursor hot-injection method with oleylamine as the sole solvent. The catalytic properties of the different phases of nickel sulfide were investigated.

EXPERIMENTAL

Materials

$Ni(NO_3)_2 \cdot 6H_2O$ (purity 98%), elemental sulfur, ethanol (99.95%), 4-nitrophenol, $NaBH_4$, and acetone (purity 99.9%) were purchased from Wako Pure Chemical Industries, Ltd., Japan. Oleylamine (70%) was purchased from Sigma Aldrich. The reagents were used without further purification.

Synthesis of Nickel Sulfide Nanoparticles

A typical procedure for nickel sulfide particle synthesis was as follows. $Ni(NO_3)_2 \cdot 6H_2O$ (1 mmol) was mixed with oleylamine (10 mL) in a 100 mL three-necked flask (A). The solution was heated at 100 °C for 1 h to remove moisture and O_2 in the oleylamine. Elemental sulfur (1 mmol) and oleylamine (10 mL) were placed in a separate 100 mL three-necked flask (B) and heated at 70 °C for 30 min to form a sulfur–amine mixture. The transparent yellow sulfur–oleylamine solution (B) was loaded into a glass syringe and injected into the nickel–oleylamine solution mixture (A). This mixture of the sources in a concentration ratio of 1:1 gave the NiS phase. The temperature was raised to 210 °C and the mixture was continually stirred for 1 h under a N_2 atmosphere to initiate the reaction. After cooling, the particles were collected by centrifugation, washed with ethanol, and dried under vacuum for 1 h. The particles were dispersed in an organic solvent and stored in a tightly closed container.

When the temperature was raised to 210 °C, the sulfur–amine mixture released H_2S, which reacted with the metal–oleylamine complex to form a nickel sulfide product[21]. These procedures were repeated using $Ni(NO_3)_2 \cdot 6H_2O$:elemental sulfur concentration ratios of 1:2, 3:4, and 3:2 to synthesize nickel sulfide nanoparticles with different phases. The oleylamine acted as both a solvent and a capping agent. Table 1

shows details of the phases present in the synthesized products with respect to concentration.

Catalytic Study

The catalytic activities of the synthesized nickel sulfide nanoparticles were investigated as follows. Aqueous solutions of 4-nitrophenol (10 mg in 50 mL of distilled water) and $NaBH_4$ (750 mg in 200 mL of distilled water) were freshly prepared. 4-Nitrophenol and $NaBH_4$ in a concentration ratio of 1:10 were mixed with nickel sulfide nanoparticles (4.0 mg). The mixture was placed in a quartz cuvette and the reaction was monitored using UV-vis spectroscopy. This step was repeated several times to study the stability of the nanoparticles.

Characterization

The crystalline phases of the final precipitates were identified by powder X-ray diffraction (XRD) performed at a scan rate of 0.04 s^{-1} in the 2θ range 10° to 80° (RINT-2200 diffractometer, Rigaku, Japan, CuKα radiation, λ = 1.54178 Å). The particle sizes and morphologies of the final precipitates were determined using transmission electron microscopy (TEM) and high-resolution TEM (HRTEM; JEOL JEM 2100F) at an accelerating voltage of 200 kV. Binding energies were investigated using X-ray photoelectron spectroscopy (XPS; Shimadzu ESCA 3100). Fourier-transform infrared spectroscopy (FTIR) was performed using a JEOL JIR-WINSPEC 50 spectrometer.

RESULTS AND DISCUSSION

NiS Phase

A typical XRD pattern of the nickel sulfide particles prepared using the temperature-dependent injection method is shown in Figure 1(a). The pattern shows that the sample is crystalline. The pattern in Figure 1(a) corresponds to the α-NiS phase. The use of a 1:1 concentration ratio of nickel to sulfur in the presence of oleylamine resulted in formation of a nickel monosulfide phase. JCPDS reference 01-075-0613, i.e., α-NiS, matched the synthesized sample well. Figure 1(b) and (c) show TEM and HRTEM images of the NiS nanoparticles. The TEM image shows that the sizes of the spherical nanoparticles ranged from 8 to 10 nm. The high-magnification image shows that the distance between the atomic layers was 2.94 Å, which matches the *d*-spacing of the (100) plane of the NiS phase (Figure 1a). A single phase with good crystallinity was obtained in a single step at 210 °C. Oleylamine helped to make the particle size distribution uniform.

NiS_2 Phase

The XRD pattern shown in Figure 2(a) matched JCPDS reference 00-011-0099, i.e., the NiS_2 phase. A source material concentration ratio of 1:2 resulted in formation of nickel disulfide nanoparticles. Figure 2(b) and (c) show the sample morphology. The TEM image shows that the cubic particles were well distributed, and of size 6–8 nm. The distance between the atomic layers of the cubic nanoparticles was 2.77 Å (Figure 2c), which matches that of the (200) plane of the NiS_2 phase.

Ni_3S_4 Phase

A concentration ratio of 3:4 (nickel source 1.5 mmol, 0.435 g; sulfur source 2 mmol, 0.064 g) gave the sulfur-rich phase Ni_3S_4. The XRD pattern, shown in Figure 3(a) matched JCPDS reference 00-047-1739 well. The TEM and HRTEM images in Figure 3(b) and (c) show that the particles had a bulging spherical morphology. The *d*-spacing observed from the HRTEM image, 2.78 Å, was close to that of the (311) plane (see Figure 3a). The *d*-spacing value of 2.33 Å corresponded to the (220) plane of the Ni_3S_4 phase.

Ni_7S_6 Phase

The XRD pattern of the material synthesized using a source concentration ratio of 3:2 matched that of the nickel-rich phase Ni_7S_6 (Figure 4a; JCPDS reference 00-014-0364). Figure 4(b) and (c) show the TEM and HRTEM images of Ni_7S_6. The TEM image shows that the well-distributed particles consisted of spherical and elongated spherical particles of size 8–20 nm. The broad particle size distribution is caused by the high nickel concentration in the source. The HRTEM image shows that the distances between the atomic layers in spherical and elongated spherical nanoparticles were different. The spherical nanoparticle *d*-spacing, 2.85 Å, corresponds to the (121) plane and the elongated spherical particle *d*-spacing, 3.12 Å, corresponds to the (042) plane.

FTIR Analysis

Figure 5 shows the FTIR spectra of the synthesized nickel sulfide nanoparticles with different phases. The peaks from the C–H stretching modes are observed at 2921 and 2852 cm^{-1}[1, 27–30], the broad peak at 3400 cm^{-1} corresponds to the N–H stretching[31] of free amines, and the peak at 1653 cm^{-1} is related to N–H rocking vibrations. The

absence of the peaks at 1389 and 3400 cm^{-1} in the spectrum of the Ni_7S_6 sample indicates lower reactivities of the C–N and N–H bonds in organic ligands[31].

XPS Analysis

The XP spectra of the different phases of the synthesized nanoparticles are shown in Figure 6. Table 2 show the binding energies of the synthesized phases. The binding energy of 852.8 eV (Ni 2p $_{3/2}$) for the NiS and Ni_7S_6 samples matched the reported values[32]. The binding energies for NiS_2 and Ni_3S_4, i.e., 852.5 and 853.1 eV, respectively, were close to the reported values of 852.85 and 854.3 eV. All the Ni $2p_{1/2}$ binding energies matched the reported values[24,33,34]. The difference between the binding energies of Ni $2p_{1/2}$ and Ni $2p_{3/2}$ is approximately equal to the standard value for nickel doublet peaks (17.4)[35], but this difference is 18.4 eV in the case of NiO bonds. This confirms that the materials are protected from oxidation by oleylamine capping of the particles. Doublet peaks of S $2p_{3/2}$ and S $2p_{1/2}$ for NiS_2, i.e., 161.2 and 162.8 eV, matched the reported NiS_2 data[33]. These values are similar to those for the nickel-rich phase Ni_7S_6. The other phases such as NiS and Ni_3S_4 had sulfur doublet peaks consistent with the reported values[32].

The different materials obtained using different molar concentrations of the source materials (Table 1) show that the availability of the nickel source for reaction with the sulfur–amine mixture is very important in synthesizing single-phase nickel sulfides. The local nickel concentration increased during the reaction to form the more stable Ni_3S_4 phase. In this case, all the sulfur source molecules reacted with the metal precursor. The complex phases in the nickel sulfide phase diagram, such as Ni_3S_4 and Ni_7S_6, were obtained without sulfur impurities. The results for the NiS and NiS_2 phases

clearly show that any stable phase of nickel sulfide can be synthesized by single-step temperature-controlled synthesis with the help of oleylamine.

Catalytic Activities of Nickel Sulfide Catalysts

We investigated the reduction of 4-nitrophenol to 4-aminophenol to help us to understand the catalytic activities of the synthesized nickel sulfide phases[36,37]. No reduction was observed without the presence of nickel sulfide catalysts. Figure 7 shows photographs of 4-nitropheneol reduction and the chemical equation. Figure 8 shows the UV-vis absorbance spectra with respect to time. During the reaction, hydrogen species were first transferred to the surface of the synthesized products and then 4-nitrophenol was reduced to 4-aminophenol[38]. In Figure 8, the absorption peak at 400 nm represents the 4-nitrophenolate ion and the peak at 293 nm is related to 4-aminophenol. When NiS nanoparticles were added to the solution, reduction to 4-aminophenol was complete in about 300 s (Figure 8a). The catalytic activities of the sulfur-rich phases were lower than that of the NiS phase. The reduction times using NiS_2 and Ni_3S_4 were both 400 s (Figure 8b and c). For the Ni_7S_6 phase, reduction was complete in 500 s. The NiS phase had much higher catalytic activity. Figure 9 shows the reduction rates with different nickel sulfide phases. The reaction rate increased linearly with respect to time. The reduction rate constant (K_{obs}) was calculated using the absorption vales for the 4-nitrophenol reduction reaction[39,40].

$$K_{\mathrm{obs}} = \frac{\ln\left[\frac{A_\infty - A_0}{A_\infty - A_t}\right]}{t}$$

where A_0, A_t, and A_∞ are the initial absorbance, absorbance at time t, and absorbance at infinite time, respectively. The calculated K_{obs} values for NiS, NiS_2, Ni_3S_4, and Ni_7S_6 are 8.949×10^{-3}, 3.030×10^{-3}, 3.728×10^{-3}, and 2.737×10^{-3} s^{-1}, respectively. Among the four synthesized nickel sulfide phases, NiS gave the highest rate of degradation of 4-nitrphenol because of its higher metallic nature[11]. To study the structural change after its catalytic reduction, nanoparticles of NiS phase were collected by centrifugation and investigated the structure by XRD analysis. Fig.10 shows the XRD pattern of NiS phase after its catalytic activity. The corresponding JCPDS reference 00-001-1286 was well matched with the NiS phase. No phase change was observed even after its catalytic reduction but the crystal system was changed from hexagonal to rhombohedral of NiS phase. The repeated catalytic activity of NiS phase was well matched with the initial experiment of Figure.8 (a) and its reduction time of 4-nitrophenol to 4-aminophenol is 300 sec.

CONCLUSIONS

We successfully synthesized nickel sulfide nanoparticles with different phases via a simple temperature-controlled injection method in oleylamine solvent. The products were uniform-sized nanocrystals. The injection method enabled the sulfur ions to react slowly with the well-dispersed nickel ions in the presence of oleylamine, to form nickel sulfide nanoparticles. This enabled formation of the desired phase instead of mixed phases. The complications in the synthesis of Ni_3S_4 were overcome by adjusting the source concentrations. XRD and TEM analyses confirmed the presence of single-phase nanoparticles of sizes less than 15 nm for all the synthesized products. The presence of sulfur and nickel and the peak shifts with respect to phase formation were observed

using XPS. The catalytic activities of the synthesized nickel sulfide nanoparticles were investigated; the NiS phase had the best activity and the phase was stable even after its catalytic reduction experiment.

ACKNOWLEDGMENTS

This work was financially supported by a Grant-in-Aid for Japan Society for the Promotion of Science (JSPS) Fellows, related to the JSPS Postdoctoral Fellowship for Foreign Researchers (No. 26 04050) from the Ministry of Education, Culture, Sports, Science, and Technology (MEXT) of Japan, and a cooperative research project of the Research Institute of Electronics, Shizuoka University. The authors would like to thank Mr. T. Koyama and Mr. W. Tomada for their help with XRD and XPS analyses. R. Karthikeyan thanks MEXT-Japan for the award of a research fellowship.

REFERENCES

1. X. Peng, L. Manna, W. Yang, J. Wickham, E. Scher, a Kadavanich, and A. Alivisatos, *Nature*, 2000, **404**, 59–61.

2. Q. Liu, A. Díaz, A. Prosvirin, Z. Luo, and J. D. Batteas, *Nanoscale*, 2014, **6**, 8935–8942.

3. C. J. Barrelet, Y. Wu, D. C. Bell, and C. M. Lieber, *J. Am. Chem. Soc.*, 2003, **125**, 11498–9.

4. Y. Hasegawa, M. Afzaal, P. O'Brien, Y. Wada, and S. Yanagida, *Chem. Commun. (Camb).*, 2005, **1**, 242–3.

5. L. Mi, Q. Ding, W. Chen, L. Zhao, H. Hou, C. Liu, C. Shen, and Z. Zheng, *Dalton Trans.*, 2013, **42**, 5724–30.

6. T. Zhu, H. Bin Wu, Y. Wang, R. Xu, and X. W. D. Lou, *Adv. Energy Mater.*, 2012, **2**, 1497–1502.

7. W. S. Chi, J. W. Han, S. Yang, D. K. Roh, H. Lee, and J. H. Kim, *Chem. Commun. (Camb).*, 2012, **48**, 9501–9503.

8. G. Kullerud and R. a. Yund, *J. Petrol.*, 1962, **3**, 126–175.

9. X. Jiang, Y. Xie, J. Lu, L. Zhu, W. He, and Y. Qian, *Adv. Mater.*, 2001, **13**, 1278–1281.

10. J. T. Sparks and T. Komoto, *J. Appl. Phys.*, 1963, **34**, 1191.

11. J. Sparks and T. Komoto, *Phys. Lett.*, 1967, **25**, 5–6.

12. J. Sparks and T. Komoto, *Rev. Mod. Phys.*, 1968, **40**, 752–754.

13. J. and J. P. R. A. S. Barker, *Phys. Rev. B*, 1974, **10**, 987–994.

14. L. Wang, Y. Zhu, H. Li, Q. Li, and Y. Qian, *J. Solid State Chem.*, 2010, **183**, 223–227.

15. S. Chen, K. Zeng, H. Li, and F. Li, *J. Solid State Chem.*, 2011, **184**, 1989–1996.

16. H. Pang, C. Wei, X. Li, G. Li, Y. Ma, S. Li, J. Chen, and J. Zhang, *Sci. Rep.*, 2014, **4**, 3577, 1–8.

17. V. G. Pol, S. V Pol, and A. Gedanken, *Adv. Mater.*, 2011, **23**, 1179–90.

18. C. N. R. Rao, S. R. C. Vivekchand, K. Biswas, and a Govindaraj, *Dalton Trans.*, 2007, 3728–49.

19. Y. H. R.Karthikeyan, M. Navaneethan, J. Archana, D. Thangaraju, M. Arivanandhan, *Dalton Trans.*, 2014, **43**, 17445–17452.

20. A. Ghezelbash and B. a Korgel, *Langmuir*, 2005, **21**, 9451–6.

21. B. Wu, N. Zheng, and G. Fu, *Chem. Commun. (Camb).*, 2011, **47**, 1039–1041.

22. S. M. Lee, Y. W. Jun, S. N. Cho, and J. Cheon, *J. Am. Chem. Soc.*, 2002, **124**, 11244–11245.

23. A. Lut, M. A. Malik, P. O. Brien, and F. Tuna, 2012, 2253–2259.

24. J. W. Thomson, K. Nagashima, P. M. Macdonald, and G. a Ozin, 2011, 3–5.

25. A. Dyal, K. Loos, M. Noto, S. W. Chang, C. Spagnoli, K. V. P. M. Shafi, A. Ulman, M. Cowman, and R. a Gross, *J. Am. Chem. Soc.*, 2003, **125**, 1684–5.

26. S. H. Choi, K. An, E. G. Kim, J. H. Yu, J. H. Kim, and T. Hyeon, *Adv. Funct. Mater.*, 2009, **19**, 1645–1649.

27. L. Polavarapu and Q.-H. Xu, *Nanotechnology*, 2009, **20**, 185606, 1–7.

28. J. He, P. Kanjanaboos, N. L. Frazer, A. Weis, X. M. Lin, and H. M. Jaeger, *Small*, 2010, **6**, 1449–1456.

29. A. Khare, A. W. Wills, L. M. Ammerman, D. J. Norris, and E. S. Aydil, *Chem. Commun.*, 2011, **47**, 11721–11723.

30. M. Klokkenburg, J. Hilhorst, and B. H. Erné, *Vib. Spectrosc.*, 2007, **43**, 243–248.

31. L. Zhang, L. Wang, Z. Jiang, and Z. Xie, *Nanoscale Res. Lett.*, 2012, **7**, 312, 1–6.

32. M. Salavati-Niasari, F. Davar, and M. Mazaheri, *Mater. Res. Bull.*, 2009, **44**, 2246–2251.

33. S.-L. Yang, H.-B. Yao, M.-R. Gao, and S.-H. Yu, *CrystEngComm*, 2009, **11**, 1383–1390.

34. L. Sangaletti, T. Thio, and J. W. Bennett, 1997, **55**, 9514–9519.

35. C. D. Wagner, W. M. Riggs, L. E. Davis, and J. F. Moulder, *Handbook of X-ray Photoelectron Spectroscopy*, 1979.

36. T. Yu, J. Zeng, B. Lim, and Y. Xia, *Adv. Mater.*, 2010, **22**, 5188–92.

37. F. H. Lin and R. A. Doong, *J. Phys. Chem. C*, 2011, **115**, 6591–6598.

38. N. Pradhan, A. Pal, and T. Pal, *Colloids Surfaces A Physicochem. Eng. Asp.*, 2002, **196**, 247–257.

39. S. Gu, S. Wunder, Y. Lu, M. Ballauff, R. Fenger, K. Rademann, B. Jaquet, and A. Zaccone, *J. Phys. Chem. C*, 2014, **118**, 18618–18625.

40. E. Murugan and J. N. Jebaranjitham, *J. Mol. Catal. A Chem.*, 2012, **365**, 128–135.

Figure captions

Figure 1. (a) XRD pattern, and (b) TEM and (c) HRTEM images of NiS phase.

Figure 2. (a) XRD pattern, and (b) TEM and (c) HRTEM images of NiS_2 phase.

Figure 3. (a) XRD pattern, and (b) TEM and (c) HRTEM images of Ni_3S_4 phase.

Figure 4. (a) XRD pattern, and (b) TEM and (c) HRTEM images of Ni_7S_6 phase.

Figure 5. FTIR patterns of different nickel sulfide phases.

Figure 6. (a) Ni 2p and (b) S 2p XP spectra of different nickel sulfide phases.

Figure 7. Catalytic reduction of 4-nitrophenol to 4-aminophenol.

Figure 8. UV-vis spectra of 4-nitrophenol reduction with (a) NiS, (b) NiS_2, (c) Ni_7S_6, and (d) Ni_3S_4 phases.

Figure 9. Effects of different nickel sulfide phases on reduction of 4-nitrophenol.

Figure. 10 XRD pattern of NiS phase after its catalytic activity

Table 1. Different concentration ratios of nickel and sulfur sources and the corresponding phases of synthesized materials

Name	Nickel source (g)	Sulfur source (g)	Concentration ratio	Phase
I – 1	0.290	0.032	1:1	NiS
I – 2	0.290	0.064	1:2	NiS_2
I – 3	0.435	0.064	3:4	Ni_3S_4
I – 4	0.435	0.032	3:2	Ni_7S_6

Table 2. XPS binding energy values

Phase	Ni $2p_{3/2}$ (eV)	Ni $2p_{1/2}$ (eV)	Ni 2p3/2 - Ni $2p_{1/2}$ (eV)	S $2p_{3/2}$ (eV)	S $2p_{1/2}$ (eV)
NiS	852.8	870.4	17.6	161.4	162.8
NiS_2	852.5	870	17.5	161.2	162.8
Ni_3S_4	853.1	870.4	17.3	161.6	162.8
Ni_7S_6	852.8	870.1	17.3	161.2	162.8

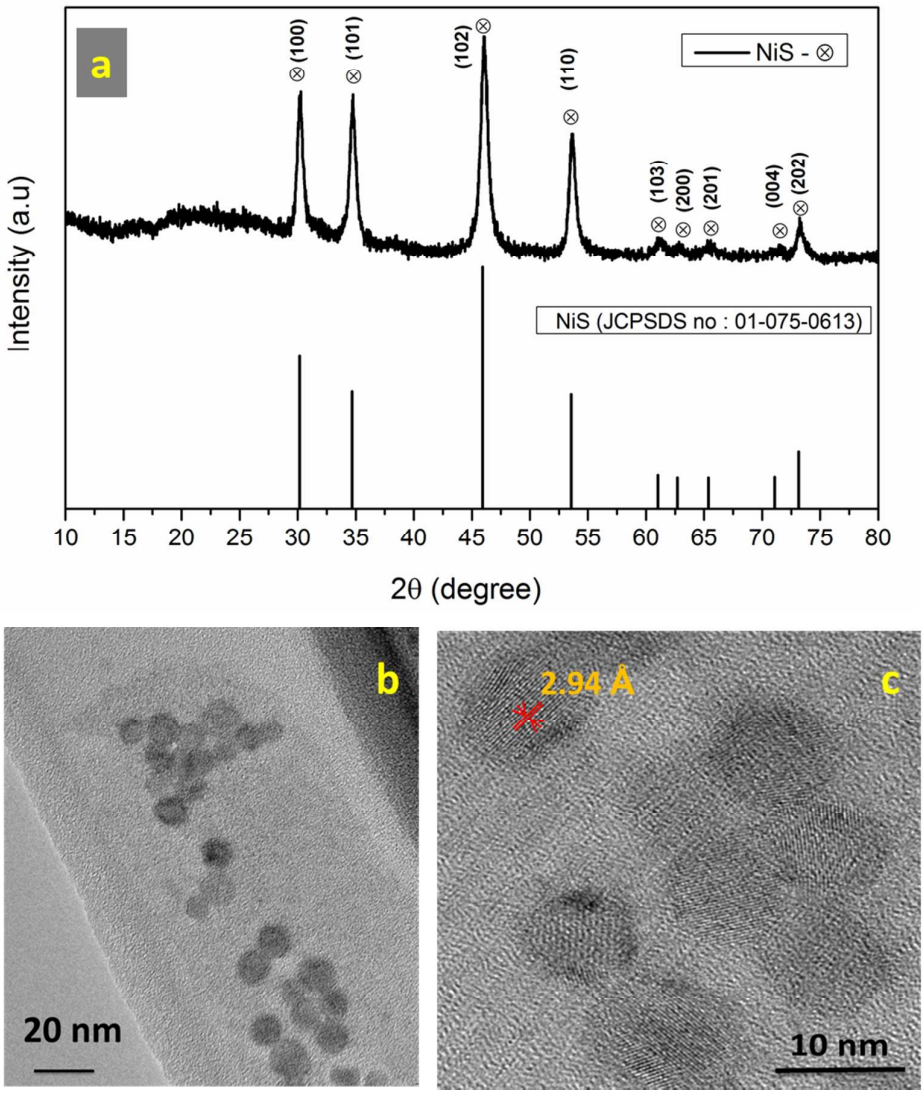

Figure 1. (a) XRD pattern, and (b) TEM and (c) HRTEM images of NiS phase.

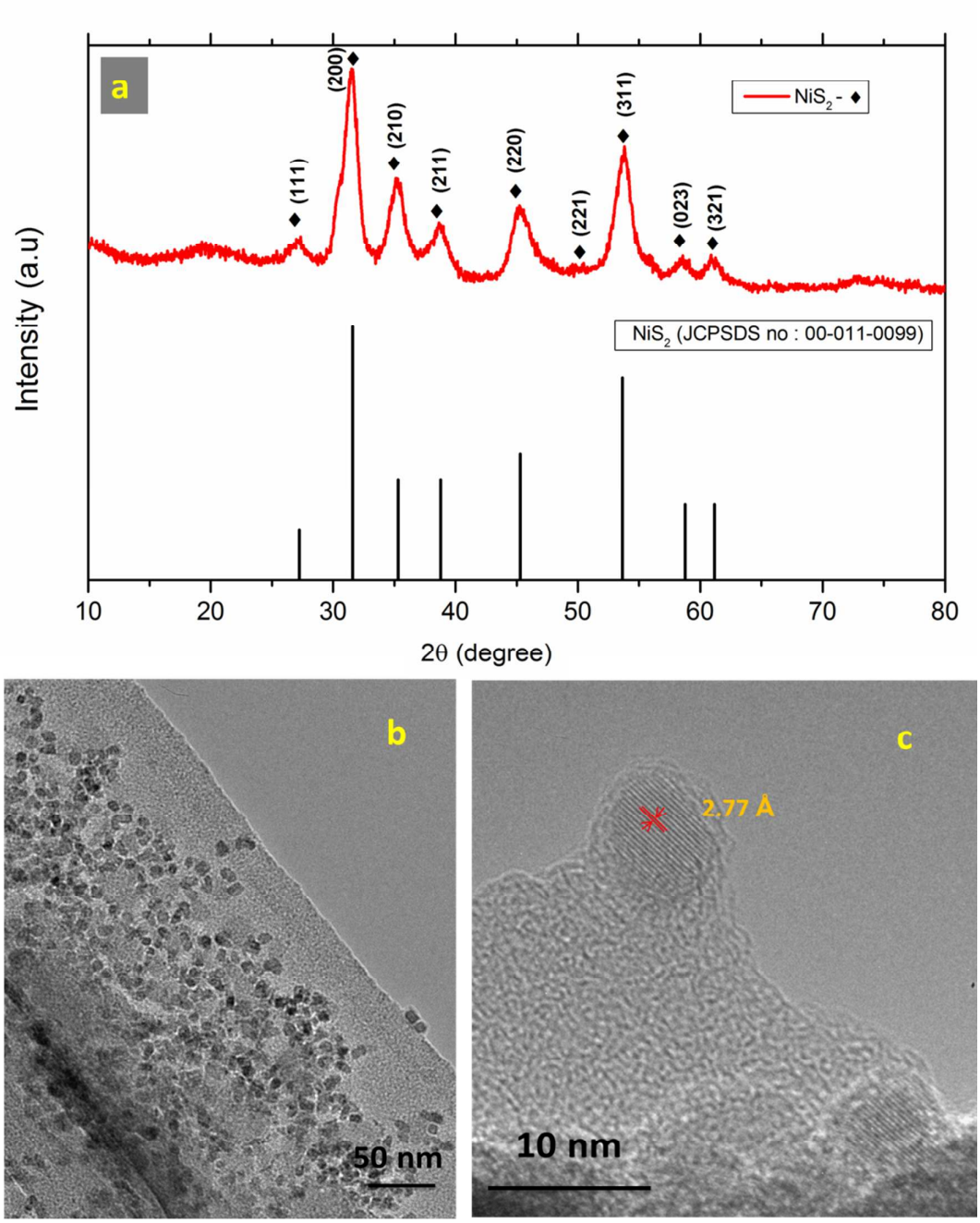

Figure 2. (a) XRD pattern, and (b) TEM and (c) HRTEM images of NiS_2 phase.

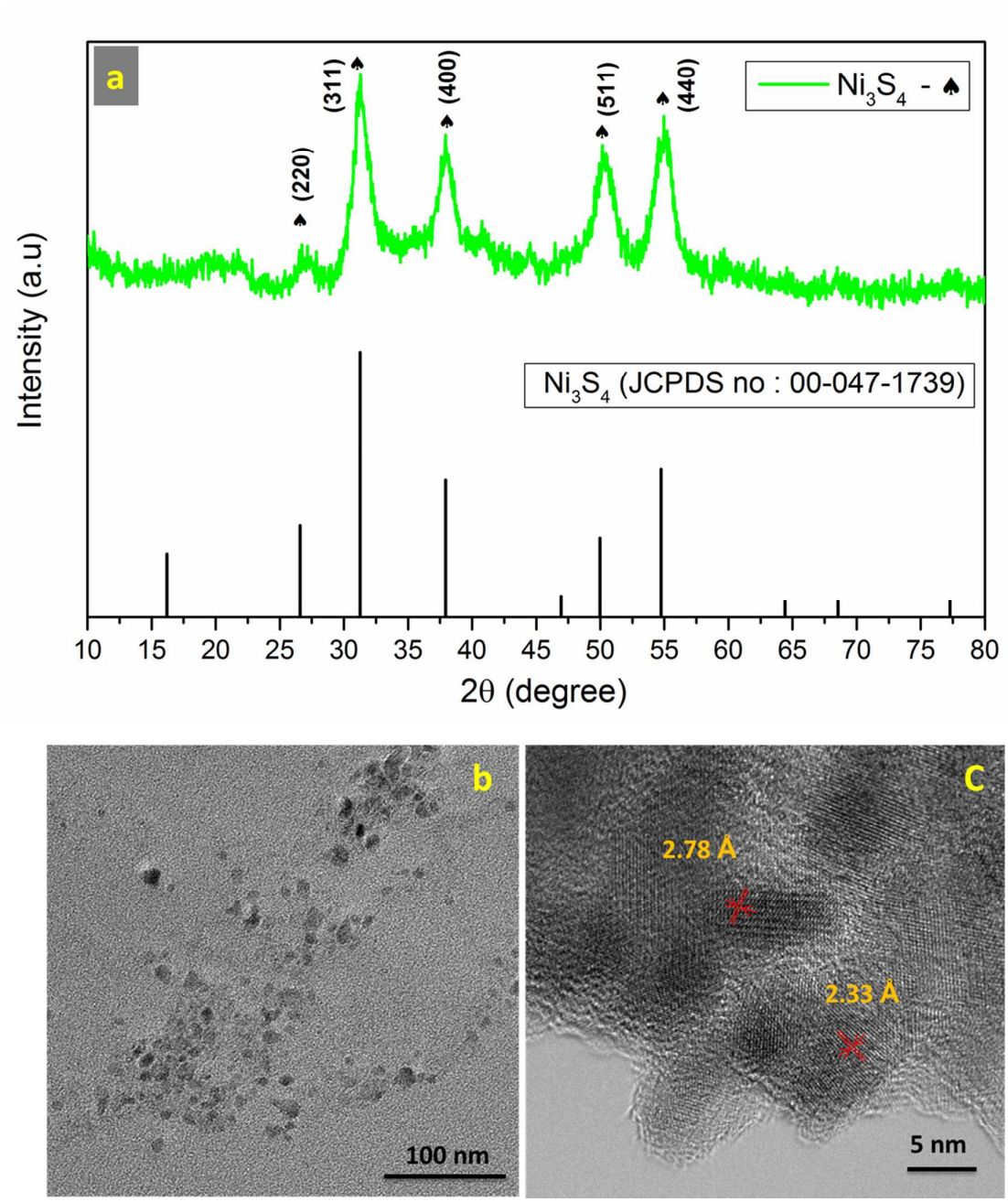

Figure 3. (a) XRD pattern, and (b) TEM and (c) HRTEM images of Ni_3S_4 phase.

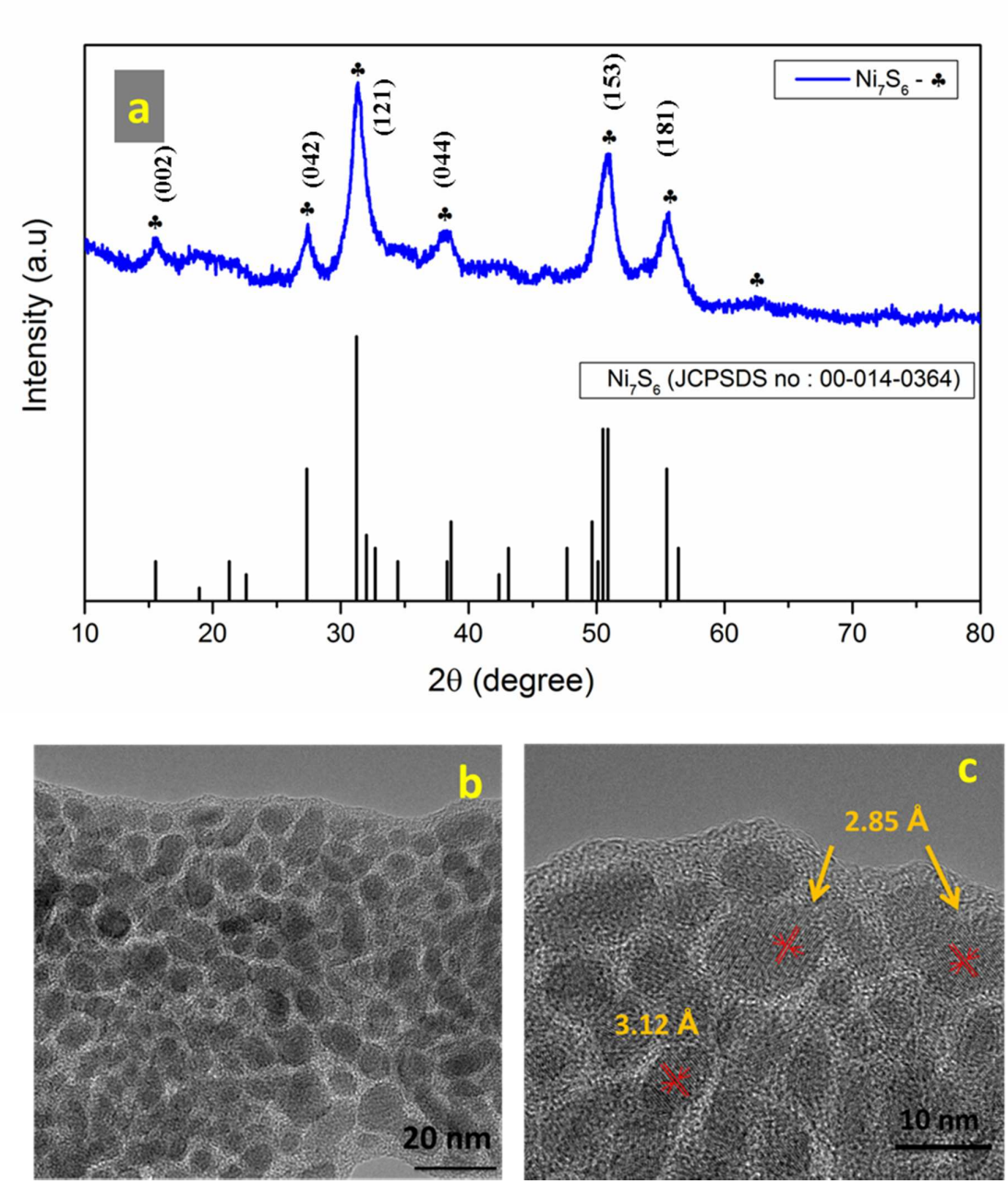

Figure 4. (a) XRD pattern, and (b) TEM and (c) HRTEM images of Ni_7S_6 phase.

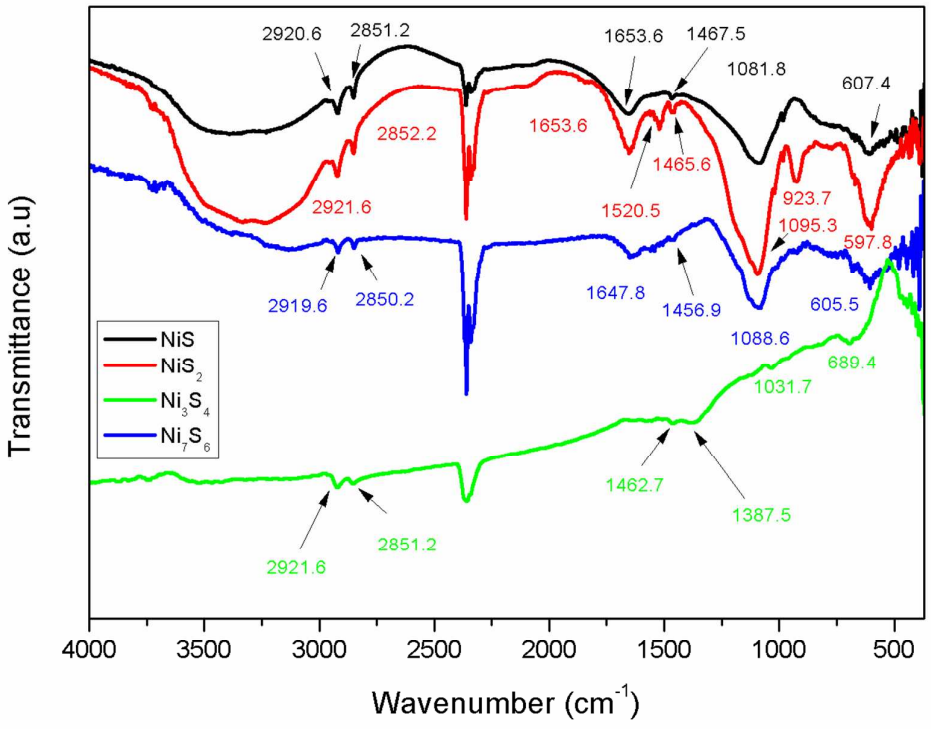

Figure 5. FTIR patterns of different nickel sulfide phases.

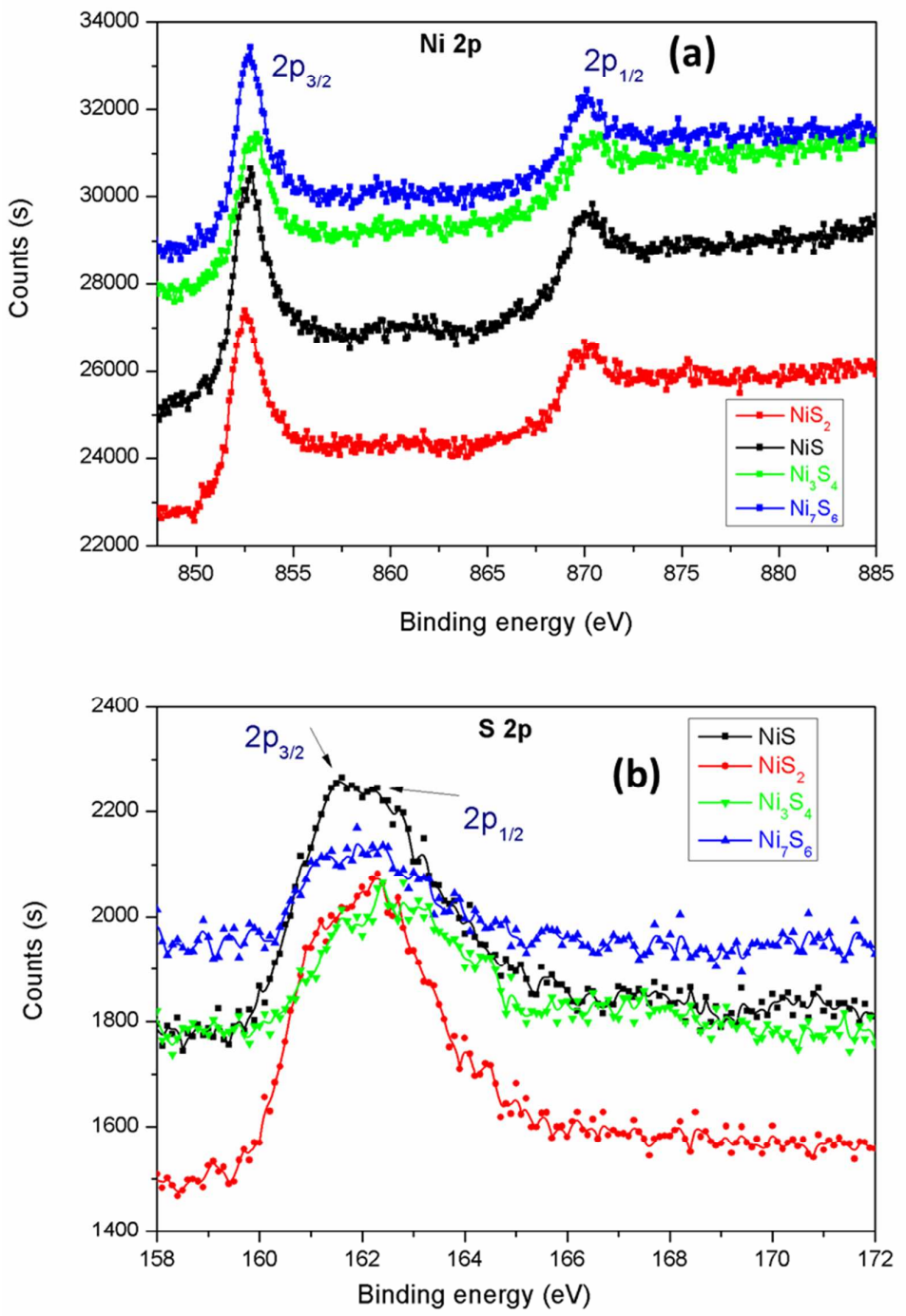

Figure 6. (a) Ni 2p and (b) S 2p XP spectra of different nickel sulfide phases.

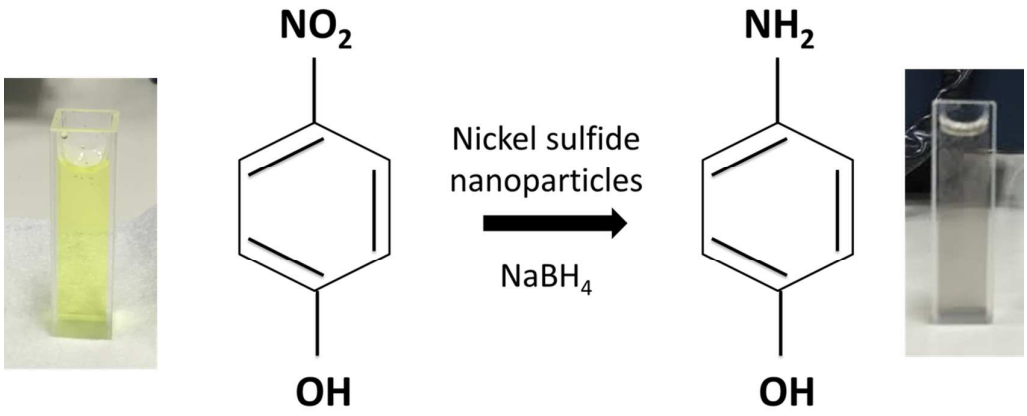

Figure 7. Catalytic reduction of 4-nitrophenol to 4-aminophenol.

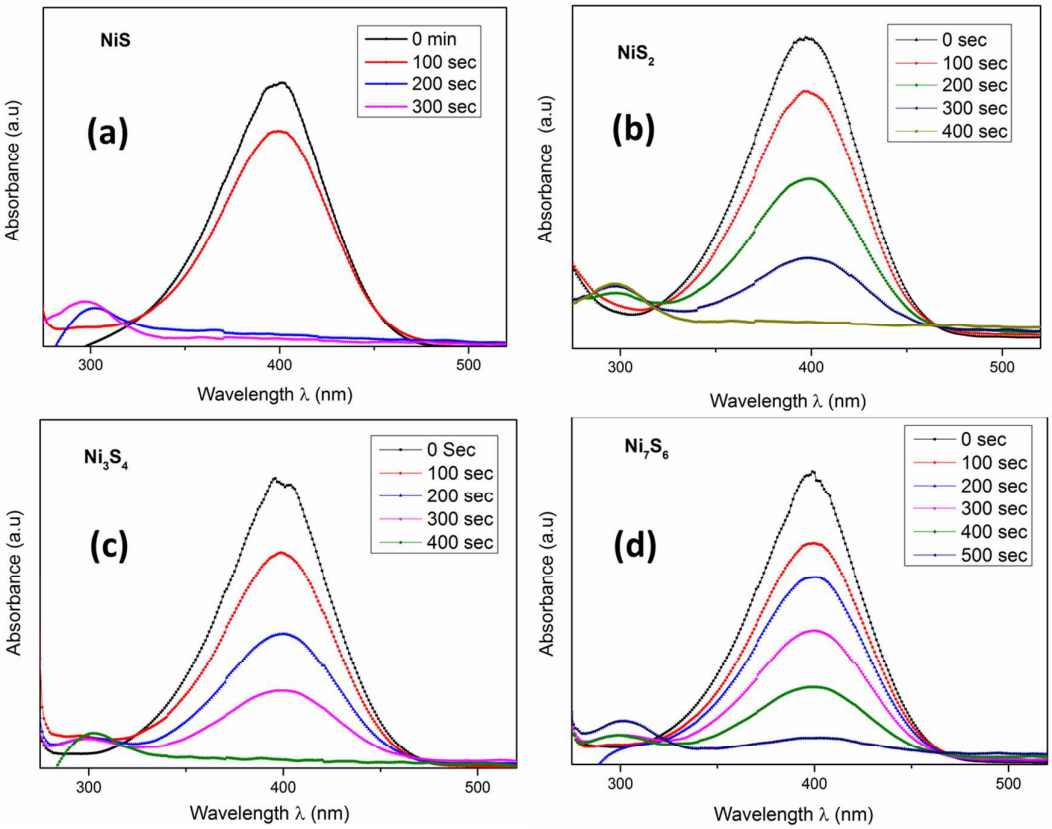

Figure 8. UV-vis spectra of 4-nitrophenol reduction with (a) NiS, (b) NiS_2, (c) Ni_7S_6, and (d) Ni_3S_4 phases.

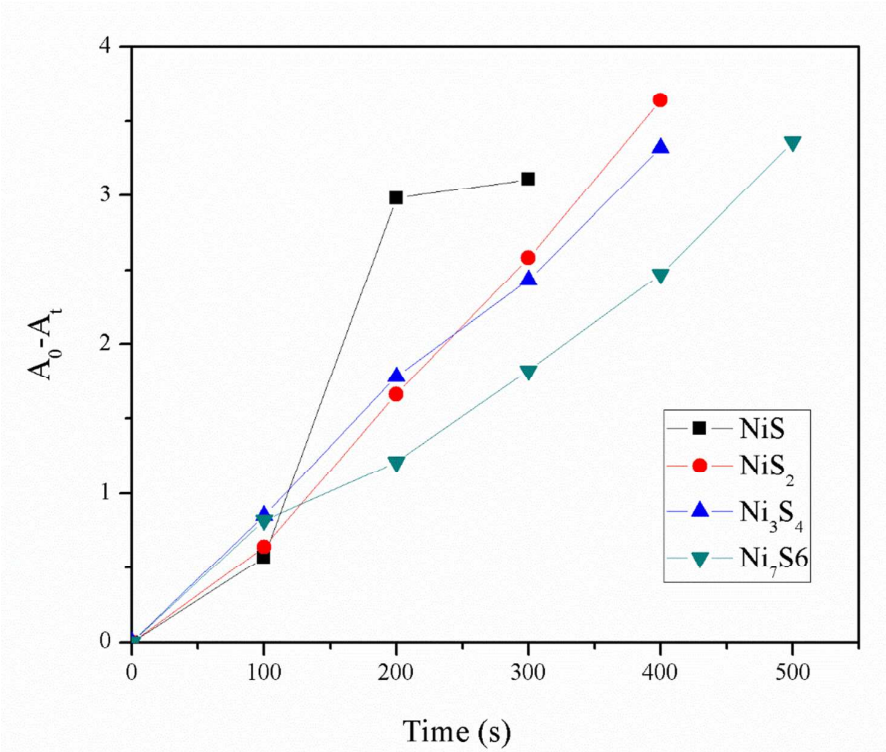

Figure 9. Effects of different nickel sulfide phases on reduction of 4-nitrophenol.

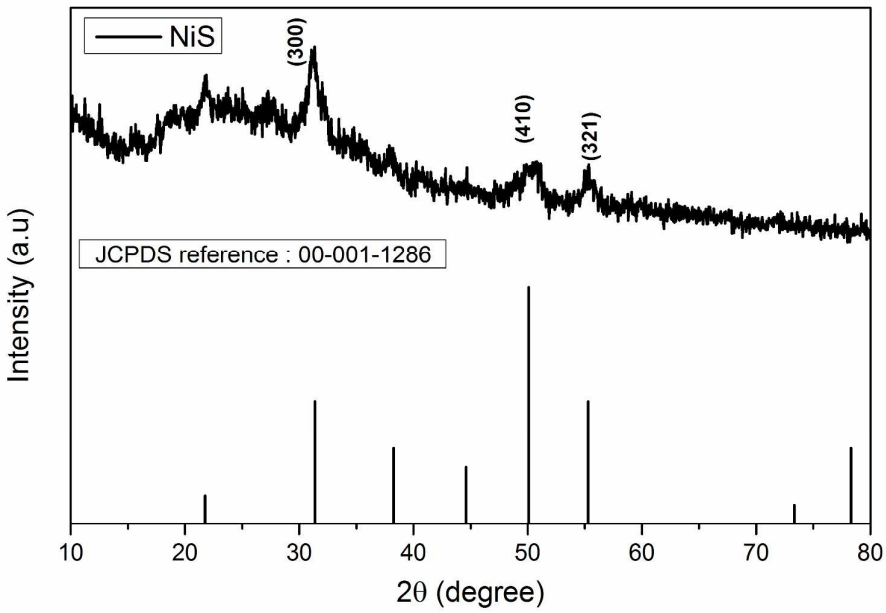

Figure. 10 XRD pattern for NiS phase after its catalytic activity